Floquet-engineered half-valley-metal state in two-dimensional gapped Dirac materials

Xikui Ma,[1] Lei Sun,[1] Jian Liu,[1,*] and Mingwen Zhao[1,2,†]
[1]*School of Physics, Shandong University, Jinan, Shandong 250100, China*
[2]*State Key Laboratory of Crystal Materials, Shandong University, Jinan, Shandong 250100, China*

(Received 7 May 2021; revised 20 October 2021; accepted 21 October 2021; published 29 October 2021)

The half-valley-metal (HVM) states where the gap of one valley is closed while the other valley remains semiconducting are quite crucial for achieving 100% valley polarization and valley-Hall-effect. However, the symmetry of materials makes the HVM states scarce. In this work, using Floquet theory, we demonstrate the laser-dressed HVM states in two-dimensional (2D) gapped-Dirac materials. We show that as a circularly polarized laser is applied to a 2D gapped-Dirac material, the gaps of the two valleys (*K* and *K*') can be regulated by varying the photon energy, amplitude and chirality of the laser. At specific photon energies and laser amplitudes, the linear energy-momentum dispersion of Dirac materials is restituted in one valley while the gap in the other valley is preserved. On the basis of first-principles calculations, we also propose a promising candidate material, boron antimonide (BSb) monolayer to achieve the laser-dressed HVM states. More interestingly, the Berry curvature in the two valleys can be tuned by changing the laser parameters.

DOI: 10.1103/PhysRevB.104.155439

I. INTRODUCTION

Recently, valley characterized as local energy extrema of the bands in momentum space, received intensive attention as a new degree of freedom of electrons. Similar to charge and spin, valley allows the constitution of binary logic states which fosters potential applications for information processing [1–6]. Extensive investigations have been focused on the valley-dependent effects such as valley polarization in monolayer group-IV transition metal dichalcogenides (TMDs), which requires a direct bandgap, inequivalent and large separation of the valleys at K and K' points in momentum space [3,7–11]. Meanwhile, the phenomenon of spin-valley locking in TMDs system demonstrates that spin and valley are coupled with each other, which excites the intersection of valleytronics and spintronics [2,7,12–15]. The demands for the generation and manipulation of valley polarization create many effective strategies, such as optical pumping [14,16,17], external field including magnetic effects [18–26] and electric effects [27–30].

Analogous to the case of spin polarization, valley polarization can also be achieved in half-valley-metal (HVM) states where the gap of one valley is closed while the other valley remains semiconducting. However, the symmetries of materials, such as the time-reversal symmetry, make the intrinsic HVM states scarce. Very recently, Duan *et al.*, demonstrated that a Dirac-type HVM state with a Dirac cone in one valley and a gap in the other valley can be formed in H-$FeCl_2$ monolayer by regulating the strength of on-site Coulomb interaction [31]. Unfortunately, regulation of on-site Coulomb interaction of materials remains challenging in experiments.

Along with the flourishing research on topological materials [32,33], researchers have found that the periodic laser field provides an additional mean to effectively manipulate the dispersion of Floquet-Bloch states in electronic systems via the coupling between electron and electromagnetic field, generating many scenarios and properties [34–38]. With the help of the model Hamiltonian and Floquet theory, various materials, such as quantum wells, quantum rings, graphene, and topological insulators [39–49] have been studied, where the periodic laser field induces topological phase transitions.

In this work, using the Floquet-Bloch theory in combination with a model Hamiltonian, we demonstrate that a circularly polarized laser can induce a photon-dressed Dirac-type HVM states in two-dimensional (2D) gapped-Dirac materials by regulating the laser energy, amplitude and chirality. On the basis of first-principles calculations, we also propose a candidate material, boron antimonide (BSb) monolayer to realize this model. Our results offer a promising strategy to achieve full spin and valley polarization in HVM states.

II. RESULTS AND DISCUSSION

A. Model of Floquet-engineered HVM state in 2D gapped Dirac materials

2D gapped Dirac materials, such as gapped graphene, boron nitride monolayer and transition-metal dichalcogenide monolayers are currently considered as the candidates for the next generation of optoelectronic devices, due to the unique electronic band structures. The electronic band lines of these materials is parabolic near the band edges but turn to linear dispersion (Dirac cone) as the band gap is closed. It has been revealed that the band gap of the gapped Dirac materials can be regulated via the interaction of electrons with a strong off-

*liujian2019phd@gmail.com
†zmw@sdu.edu.cn

resonant electromagnetic field [39]. In this work, we describe the electronic band structure of a 2D gapped Dirac material in the proximity of Fermi level using a two-band Hamiltonian for the spinless case [39]:

$$H = \begin{pmatrix} m_1 + \tau\lambda_c & \tau k_x - ik_y \\ \tau k_x + ik_y & m_2 - \tau\lambda_v \end{pmatrix}, \quad (1)$$

where m_1 and m_2 are the mass terms which serve as the source of gap, $\lambda_{c,v}$ is the spin-orbit splitting of the conduction (valence) band, $\tau = \pm 1$ is the valley index which corresponds to the two valleys at the corners of the Brillouin zone (K and K'), and $\boldsymbol{k} = (k_x, k_y)$ is the wave vector relative to the K and K' points.

When an electromagnetic field is applied, the properties of dressed electrons can be described by the Hamiltonian:

$$H(\boldsymbol{k}) = \begin{pmatrix} m_1 + \tau\lambda_c & \tau(k_x + A_x) - i(k_y + A_y) \\ \tau(k_x + A_x) + i(k_y + A_y) & m_2 - \tau\lambda_v \end{pmatrix}, \quad (2)$$

which is obtained by making Peierls substitution $\boldsymbol{k} \to \boldsymbol{k} + \boldsymbol{A}$ in Eq. (1). $\boldsymbol{A} = (A_x, A_y, 0)$ is the vector potential of the electromagnetic field. Here, the dressing field is assumed to be a left-handed circularly polarized laser (CPL) in the xy plane with the vector potential of $\boldsymbol{A} = A(\cos(\omega t), \sin(\omega t), 0)$. The intensity of the laser can be correlated to the photon energy ($\hbar\omega$) and laser amplitude (A) [39]. When the laser frequency ω is far from all resonant frequencies of electronic system, photons cannot be absorbed by electrons near the band edge. In this case, Eq. (2) can be approximated to an effective Hamiltonian [40,50], which reads

$$H_{\text{eff}} = H_0 + \frac{[H_{+1}, H_{-1}]}{\hbar\omega}. \quad (3)$$

The photon dressed Hamiltonians H_0 and $H_{\pm 1}$ can be obtained with $H_n = \frac{1}{T}\int_0^T H(\boldsymbol{k})e^{in\omega t}dt$, where T is the periodicity and $\hbar\omega$ is the photon energy of the CPL.

The time-dependent Hamiltonian can be reduced to the static equation $H_{\text{eff}}\Psi = E\Psi$ with the eigenvalues of

$$E_{\pm} = \frac{m_1^A + m_2^A \pm \sqrt{\left(m_1^A - m_2^A\right)^2 + 4\left(k_x{}^2 + k_y{}^2\right)}}{2}, \quad (4)$$

where $m_1^A = m_1 + \tau(\lambda_c - \frac{A^2}{\hbar\omega})$ and $m_2^A = m_2 - \tau(\lambda_v - \frac{A^2}{\hbar\omega})$. The renormalized band gap of the gapped Dirac materials in K and K' valleys ($k_x = k_y = 0$) dressed by a CPL can be written as

$$\Delta = \left| m_1' - m_2' - 2\tau\frac{A^2}{\hbar\omega} \right|, \quad (5)$$

where $m_1' = m_1 + \tau\lambda_c$ and $m_2' = m_2 - \tau\lambda_v$. $\Delta^0 = m_1' - m_2'$ is the intrinsic band gap in the two valleys. Clearly the dressed band gap at the two valleys exhibit different variation trends as a function of amplitude A, as shown in Fig. 1(a). The band gap at the K' ($\tau = -1$) valley increases monotonously with increasing amplitude A, whereas the band gap at the K ($\tau = 1$) valley decreases to zero and then increases. The critical point of closing the band gap at the K valley is determined by the equation:

$$A = \sqrt{2\Delta^0\hbar\omega}. \quad (6)$$

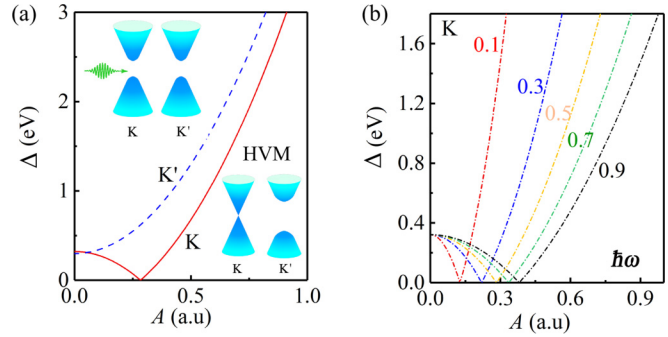

FIG. 1. Variation of the band gaps at the K and K' points under circularly polarized laser as a function of amplitude and photon energy of the laser obtained from the effective Hamiltonian of Eq. (5). (a) The photon energy is set to $\hbar\omega = 0.5\ eV$. The half-valley-metal (HVM) state emerges as the band gap at the K point is closed. (b) The dependence of the band gaps on the photon energy varying from 0.1 to 0.9 eV and the amplitude. The parameters are set to $m_1 = -m_2 = 0.155$, $\lambda_v = 0.0065$ and $\lambda_c = 0.005$.

Notably, accompanied by the close of the band gap at the K valley, a linear energy dispersion (half-Dirac cone) emerges, according to Eq. (4), giving rise to the Dirac-type HVM state [31]. The critical laser amplitude increases with the increase of the photon energy of the CPL, as shown in Fig. 1(b). Apart from the HVM state, the difference of band gap between the two valleys (referred to as valley splitting) is also greatly enhanced by the dressed CPL, which is beneficial for achieving the valley Hall effect. The band gap evolution of the two valleys reverses, as a right-handed CPL is applied. It should be stressed that Eq. (6) does not work for low photon energy ($\hbar\omega < \Delta^0$), because the high order terms of $1/\omega$ are excluded.

B. Floquet-engineered HVM state in BSb monolayer

To achieve the laser-dressed HVM state described in the above model, we consider a 2D hexagonal boron antimonide (BSb) monolayer by means of first-principles calculations. BSb monolayer has the same lattice structure as hexagonal BN monolayer, except the different bond length and lattice constant, as shown in Fig. S1 [50]. Our calculations show that the lattice constant of BSb monolayer is 3.74 Å and the bond length between B and Sb atoms is 2.16 Å, which are in good agreement with the results of a previous work (lattice parameter is 3.68 Å and bond length is 2.12 Å) [51]. The absence of imaginary frequencies in phonon spectrum demonstrates the stability of BSb monolayer [51].

Figure 2(a) plots the orbital-projected band structures of the BSb monolayer without spin-orbit coupling (SOC) effect. It is clear that BSb monolayer exhibits the valley-shaped dispersion near K (and K') point. The band gap (334 meV) is much smaller than that of the BN monolayer, due to the small electronegativity of Sb atom compared with N atom. The valence band maximum (VBM) and conduction band minimum (CBM) are mainly contributed by the p_z orbitals of B and Sb atom, respectively, which is further verified by the spatial distribution of the Kohn-Sham electron wave functions of CBM and VBM plotted in Figs. 2(c) and 2(d).

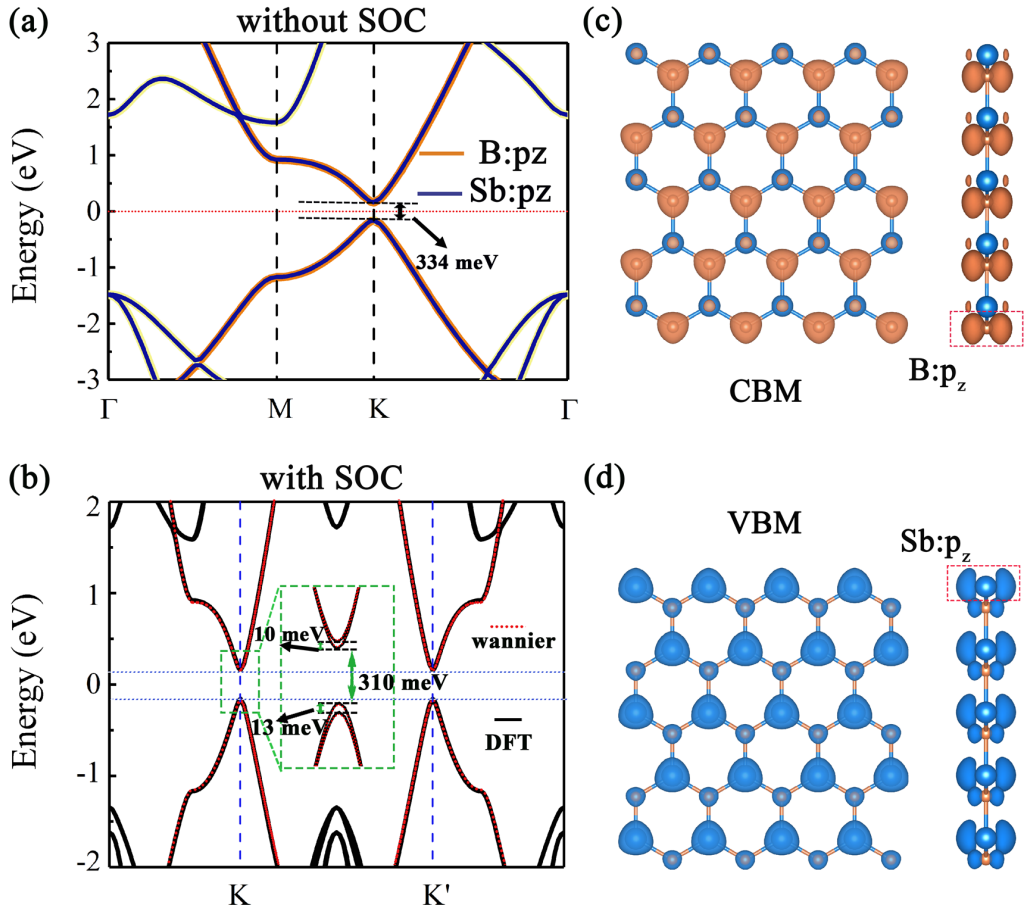

FIG. 2. (a) Electronic band structures of BSb monolayer without SOC. The Fermi level is set to zero. The orange and pale blue in band structure represent the contribution of B $-$ p_z orbitals and Sb $-$ p_z orbitals. (b) Electronic band structure of BSb monolayer with SOC. The black solid line and red dotted line represent the results from DFT calculation and Wannier fitting, respectively. (c) and (d) The electron wave functions of conduction band maximum and valence band maximum of BSb monolayer.

When the SOC effect is involved, spin splitting emerges near the K and K' points, as shown in Fig. 2(b), due to the heavy Sb atom. The magnitudes of the spin splitting are about 13 meV (for VBM) and 10 meV (for CBM), which reduce the band gap of the BSb monolayer to 310 meV. The electronic energy spectrum of the BSb monolayer in the two valleys can also be fitted by using the two-band Hamiltonian of Eq. (1) with $m_1 = 0.155$, $m_2 = -0.155$, $\lambda_v = 0.0065$, and $\lambda_c = 0.005$. Notably, the spins of the VBM (and CBM) at the K and K' valleys of the noncentrosymmetry BSb monolayer are opposite due to the time-reversal symmetry. This spin-valley locking effect offers a promising approach for spin manipulation.

The Floquet-Bloch band structures of the BSb monolayer dressed by CPL were then calculated by using the Wannier functions and Floquet-Bloch theory. We construct the effective Hamiltonian ($H^W(\boldsymbol{k})$) in the Wannier basis with p_z orbital of every B and Sb atom as projected orbitals. As shown in Fig. 2(b), the band structures from Wannier functions agree well with those of the first-principles results, which guarantees the validity of the Hamiltonian.

According to the Floquet theorem, the effect of time-periodic laser field is treated by the Peierls substitution

$$H^W(\boldsymbol{k}) \to H^W(\boldsymbol{k}, t) = H^W(\boldsymbol{k} + \boldsymbol{A}(t)), \tag{7}$$

where $\boldsymbol{A}(t)$ is the time-dependent vector potential of the applied laser field. Based on the Wannier basis, the Floquet Hamiltonian $H_F^W(\boldsymbol{k})$ with fifth order ($n = -2,-1,\ 0,\ 1,2$), which is enough to be convergent, is rewritten as [47]

$$H_F^W(\boldsymbol{k}) = \begin{bmatrix} \ddots & \vdots & \vdots & \vdots & \vdots \\ \cdots & H_{-1,-1} + I\omega & H_{-1,0} & H_{-1,1} & \cdots \\ \cdots & H_{0,-1} & H_{0,0} & H_{0,1} & \cdots \\ \cdots & H_{1,-1} & H_{1,0} & H_{1,1} - I\omega & \cdots \\ \vdots & \vdots & \vdots & \vdots & \ddots \end{bmatrix}, \tag{8}$$

where the $H_{m,n}$ is a static Hamiltonian and can be written as

$$H_{m,n} = \frac{1}{T}\int_0^T e^{i(m-n)\omega t} H^W(\boldsymbol{k}, t)dt, \tag{9}$$

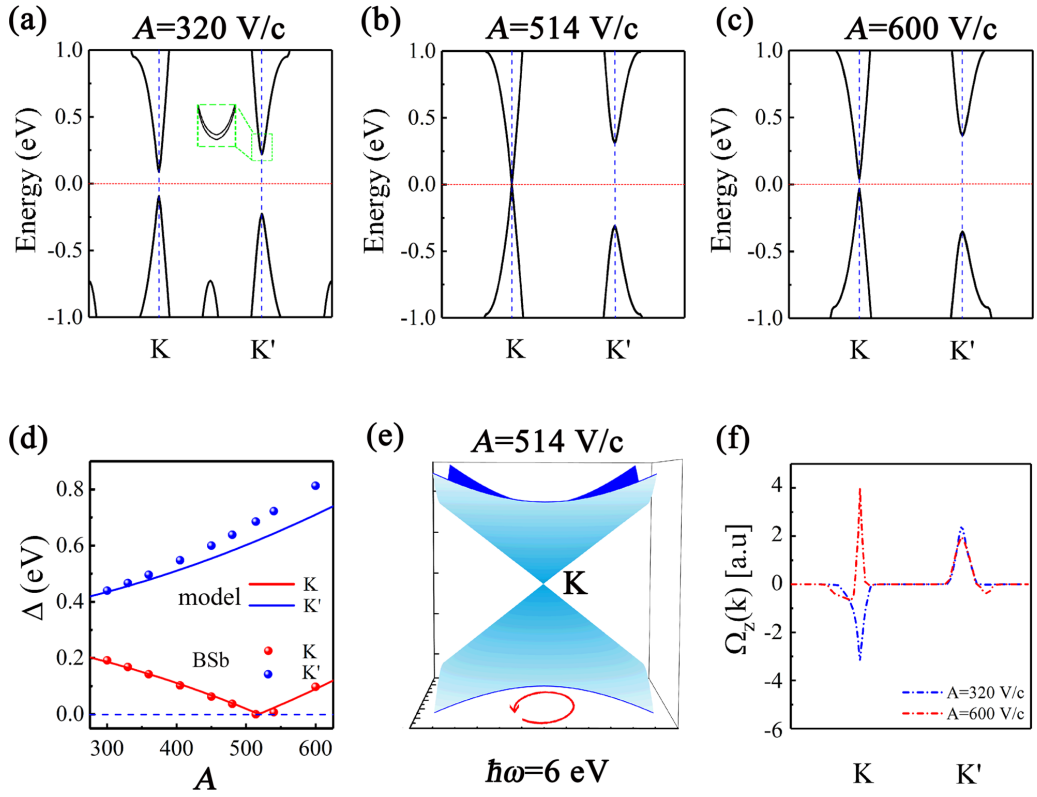

FIG. 3. (a)–(c) Band structures of BSb monolayer around K and K' valley near Fermi level under the left-handed CPL with amplitudes of 320 V/c, 514 V/c and 600 V/c and phonon energy of 6 eV, respectively. (d) The variation of bandgap at the K and K' valley as a function of amplitude. The solid lines represent the result from the model. The dots represent the result from BSb monolayer. (e) Three-dimensional band structure near the K point with $A = 514\,\mathrm{V/c}$. (f) The renormalized Berry curvature around K and K' with different amplitudes.

where the integers m and n define the Hilbert space [40]. The Floquet-Bloch band structures can be obtained by diagonalizing $H_F^W(\boldsymbol{k})$.

In our calculations, we adopted a left-handed CPL with the time-dependent vector potential of $\boldsymbol{A} = A(\cos(\omega t), \sin(\omega t), 0)$ to address the electronic band structures of the BSb monolayer. The CPL can mix the photon-dressed Floquet side bands to reach the possibility of realizing the HVM state. Under the irradiation of the CPL, the time-reversal symmetry is broken in the BSb monolayer, which lifts the degeneracy of the K and K' valleys. Therefore, the band gaps of the two valleys exhibit different evolution with the increase of laser amplitude, as shown in Figs. 3(a)−3(d). Such a difference can be regarded as the result of optical Stark effect [46]. In order to show the band evolution near the critical point more clearly, we adopted a large off-resonance photon energy of 6 eV in these figures. As laser amplitude increases to ∼514 V/c (c is the velocity of light), the band gap at the K valley vanishes, while the K' valley remains gapped, as shown in Fig. 3(b). When the laser amplitude further increases, the band gap at the K valley is reopened and increases with the increase of laser amplitude, as shown in Figs. 3(c) and 3(d). Notably, the variation of band gaps of the two valleys obtained from the density functional theory (DFT) calculations can be well fitted by using Eq. (6), as shown in Fig. 3(d), demonstrating the reliability of our model without high order terms of $1/\omega$. Accompanied by the closing of the band gap at the K valley, a linear energy dispersion (Dirac cone) emerges, as shown in Fig. 3(e). These results are in good agreement with the predictions of our simple model. Notably, the Dirac-type HVM state in the BSb monolayer allows the conducting electrons to be fully spin and valley polarized, which offers a promising platform for manipulating the spin and valley degrees of freedoms.

In the equilibrium state (without CPL), BSb monolayer has nonzero Berry curvature in the region near the valleys, but the Berry curvature in the K and K' valleys has the opposite signs due to the time-reversal symmetry. We evaluate the Floquet-engineered Berry curvature near the two valleys by supposing the Fermi occupation function of the laser-dressed BSb monolayer is close to that of the equilibrium state. From Fig. S2 [50] and Fig. 3(f), one can find that the two valleys have the opposite Berry curvature when the laser amplitude is smaller than the critical point, similar to the case of the equilibrium state. However, when the laser amplitude exceeds the critical point, accompanied by the reopening of the band gap at the K valley, the sign of the Berry curvature at the K valley reverses. Similar results have also been found in Floquet-engineered twisted bilayer graphene [49]. The fully spin-valley-polarized carriers of the HVM state may be promising in realizing spin-valley Hall effect without the need of vertical magnetic field.

Floquet-engineered electronic band structures at the two valleys are highly dependent on the chirality of CPL. For a right-handed CPL, the evaluation of band gaps and Berry curvature at the K and K' valleys exchanges, i.e., band gap closing (and reopening) and the reverse of Berry curvature

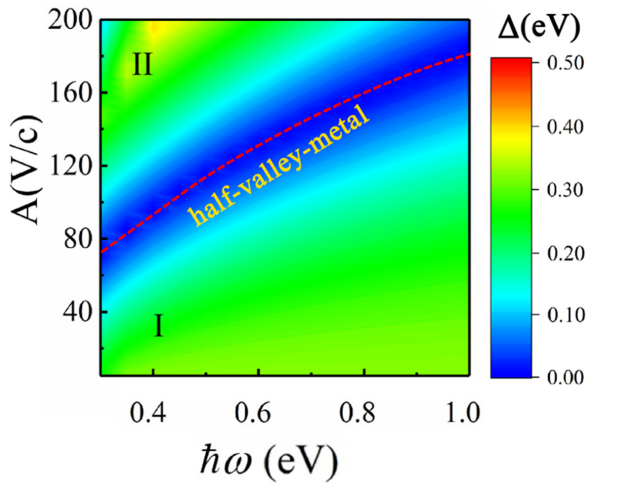

FIG. 4. Dependence of the band gap of BSb monolayer in the K valley on the photon energy E, and amplitude A. The half-valley-metal state is marked by red dashed lines.

occurs at the K' valley, as shown in Fig. S3 [50]. The tunable Berry curvature in the photon-dressed BSb monolayer holds great promise in valleytronics devices.

The Floquet-engineered band gap at the K valley (under a left-handed CPL) of the BSb monolayer as function of laser amplitude and photon energy is plotted in Fig. 4. The phase diagram can be divided into two regions. In region I, the two valleys have opposite Berry curvature and the band gap at the K point decreases with the increase (or decrease) of laser amplitude (or photon energy). In the region II, the band gap of the K valley is reopened and increases with the increase (or decrease) of laser amplitude (or photon energy), and the sign of the Berry curvature in the K valley reverses. The two valleys have the same signs of Berry curvature. The interface between the two regions corresponds to the half-Dirac HVM state determined by Eq. (6). The larger the laser energy, the greater the laser amplitude is required to realize the HVM state, which agrees with the previous Hamiltonian model in Fig. 1(b). The band gap in the K' valley increases with the increase of laser amplitude in the whole region. The laser-dressed HVM state can lead to fully spin-valley-polarized currents where the carriers coming from a single valley and a single spin channel.

It is worth mentioning that accompanied by the reversion of the Berry curvature in the K valley, a topologically nontrivial state is expected in region II, because the two valleys have the same sign of Berry curvature. However, from our present calculations, the corresponding state is still topologically trivial. We notice the small negative Berry curvature regions near the two valleys, as shown in Fig. 3(f), which can be attributed to the abnormal peak occur near the K' valley, as shown in Fig. S4 [50]. The two abnormal negative Berry curvature regions may offset the positive Berry curvature in the whole Brillouin zone.

Finally, we should stress that we adopt a high photon energy of 6.0 eV to show the HVM more clearly in Fig. 3. Actually, according to Eq. (6) and Fig. 4, HVM state can also be achieved under lower photon energy. For $\hbar\omega = 0.6$ eV, this corresponds to the amplitude A of 36.5 V/m, and the laser intensity that can induce HVM state in BSb monolayer is only about 0.18×10^{11} W/cm^2, which is in the same order of the laser employed in a previous literature [40]. This intensity is very low and will not heat the BSb monolayer. Additionally, adopting short intermediate timescales can also suppress the possible heating rate [52].

III. CONCLUSIONS

In summary, we demonstrate that the coupling between valley and electromagnetic field can lead to the HVM state in the Floquet-engineered 2D gapped Dirac materials. The HVM state obtained at specific photon energy and laser amplitude has a linear energy dispersion (half-Dirac cone) in one valley but a band gap in another valley, which guarantees 100% valley and spin polarization. Taking the BSb monolayer as an example, we give the phase diagram of the Floquet-engineered electronic structures by using first-principles calculations and Floquet-Bloch theory. Our calculations show that under a circularly polarized laser, the band gap in one valley decreases with the increase of laser amplitude and vanishes at a critical point, while the band gap in the other valley increases monotonously with the increase of laser amplitude. Accompanied by the close of the band gap at the critical point, a linear energy dispersion (Dirac cone) emerges in the valley. Further increase of the laser amplitude, the band gap is reopened along with the reversion of the Berry curvature in the valley. The laser-dressed half-Dirac HVM state in the gapped Dirac materials offers a promising platform for the generation and manipulation of spins and valleys in valleytronics devices.

ACKNOWLEDGMENTS

This study is supported by the National Natural Science Foundation of China (No. 12074218), the Special Foundation for Theoretical Physics Research Program of China (No. 11947207), the China Postdoctoral Science Foundation (No. 2020M672039), and the Taishan Scholar Program of Shandong Province.

APPENDIX: DETAILS FOR FIRST-PRINCIPLES CALCULATIONS

The first-principles calculations were performed in the Vienna *ab initio* simulation package (VASP) with projector augmented wave method in the framework of DFT [53–55]. The generalized gradient approximation with Perdew-Burke-Ermzer was applied to describe the interaction between valence electrons and ionic cores [56,57]. All the atoms were fully relaxed without any symmetry restriction until the residual forces on each atom are smaller than 0.01 eV/Å. The criterion for energy convergence is 10^{-6} eV/cell. The energy cutoff of the plane waves was chosen as 500 eV [58]. The Brillouin zone integration was sampled by an $11 \times 11 \times 1$ k-grid mesh for calculation. A large vacuum space of 20 Å was applied along the z direction to avoid interaction between adjacent images.

[1] D. Xiao, W. Yao, and Q. Niu, Phys. Rev. Lett. **99**, 236809 (2007).
[2] W. Yao, D. Xiao, and Q. Niu, Phys. Rev. B **77**, 235406 (2008).
[3] T. Cao, G. Wang, W. Han, H. Ye, C. Zhu, J. Shi, Q. Niu, P. Tan, E. Wang, and G. B. Liu, Nat. Commun. **3**, 887 (2012).
[4] X. Li, T. Cao, Q. Niu, J. Shi, and J. Feng, Proc. Natl. Acad Sci. **110**, 3738 (2013).
[5] S. Wu, J. Ross, G. Liu, G. Aivazian, A. Jones, Z. Fei, W. Zhu, D. Xiao, W. Yao, D. Cobden, and X. Xu, Nat. Phys. **9**, 149 (2013).
[6] G. Aivazian, Z. Gong, A. Jones, R. Chu, J. Yan, D. Mandrus, C. Zhang, D. Cobden, W. Yao, and X. Xu, Nat. Phys. **11**, 148 (2015).
[7] D. Xiao, G. B. Liu, W. Feng, X. Xu, and W. Yao, Phys. Rev. Lett. **108**, 196802 (2012).
[8] H. Zeng, J. Dai, W. Yao, D. Xiao, and X. Cui, Nat. Nanotechnol. **7**, 490 (2012).
[9] X. Liu, X. Ma, H. Gao, X. Zhang, H. Ai, W. Li, and M. Zhao, Nanoscale **10**, 13179 (2018).
[10] X. Ma, H. Ai, H. Gao, X. Zhang, W. Li, and M. Zhao, Phys. Chem. Chem. Phys. **21**, 3954 (2019).
[11] K. F. Mak, K. He, J. Shan, and T. F. Heinz, Nat. Nanotechnol. **7**, 494 (2012).
[12] K. F. Mak, K. L. McGill, J. Park, and P. L. McEuen, Science **344**, 1489 (2014).
[13] X. Xu, W. Yao, D. Xiao, and T. F. Heinz, Nat. Phys. **10**, 343 (2014).
[14] A. M. Jones, H. Yu, N. J. Ghimire, S. Wu, G. Aivazian, J. S. Ross, B. Zhao, J. Yan, D. G. Mandrus, D. Xiao, W. Yao, and X. Xu, Nat. Nanotechnol. **8**, 634 (2013).
[15] A. Kuc and T. Heine, Chem. Soc. Rev. **44**, 2603 (2015).
[16] A. Srivastava, M. Sidler, A. V. Allain, D. S. Lembke, A. Kis, and A. Imamoğlu, Nat. Phys. **11**, 141 (2015).
[17] K. L. Seyler, D. Zhong, B. Huang, X. Lin, N. P. Wilson, T. Taniguchi, K. Watanabe, W. Yao, D. Xiao, M. A. McGuire, K. C. Fu, and X.Xu, Nano Lett **18**, 3823 (2018).
[18] Y. C. Cheng, Q. Y. Zhang, and U. Schwingenschlögl, Phys. Rev. B **89**, 155429 (2014).
[19] D. MacNeill, C. Heikes, K. F. Mak, Z. Anderson, A. Kormanyos, V. Zolyomi, J. Park, and D. C. Ralph, Phys. Rev. Lett. **114**, 037401 (2015).
[20] J. Qi, X. Li, Q. Niu, and J. Feng, Phys. Rev. B **92**, 121403(R) (2015).
[21] Q. Zhang, S. A. Yang, W. Mi, Y. Cheng, and U. Schwingenschlogl, Adv. Mater. **28**, 959 (2016).
[22] W. Y. Tong, S. J. Gong, X. Wan, and C. G. Duan, Nat. Commun. **7**, 13612 (2016).
[23] X. Liang, L. Deng, F. Huang, T. Tang, C. Wang, Y. Zhu, J. Qin, Y. Zhang, B. Peng, and L. Bi, Nanoscale **9**, 9502 (2017).
[24] J. Liu, W.-J. Hou, C. Cheng, H.-X. Fu, J.-T. Sun, and S. Meng, J. Phys.: Condens. Matter **29**, 255501 (2017).
[25] M. Bonilla, S. Kolekar, Y. Ma, H. C. Diaz, V. Kalappattil, R. Das, T. Eggers, H. R. Gutierrez, M. Phan, and M. Batzill, Nat. Nanotechnol. **13**, 289 (2018).
[26] Q. Pei, B. Zhou, W. Mi, and Y. Cheng, ACS Appl. Mater. Interfaces **11**, 12675 (2019).
[27] Y. Ye, J. Xiao, H. Wang, Z. Ye, H. Zhu, M. Zhao, Y. Wang, J. Zhao, X. Yin, and X. Zhang, Nat. Nanotechnol. **11**, 598 (2016).
[28] Q. Pei and W. Mi, Phys. Rev. Appl. **11**, 014011 (2019).
[29] X. Ma, L. Sun, J. Liu, X. Feng, W. Li, J. Hu, and M. Zhao, Phys. Status Solidi RRL **14**, 2000008 (2020).
[30] X. Ma, X. Shao, Y. Fan, J. Liu, X. Feng, L. Sun, and M. Zhao, J. Mater. Chem. C **8**, 14895 (2020).
[31] H. Hu, W.-Y. Tong, Y.-H. Shen, X. Wan, and C.-G. Duan, npj Comput. Mater. **6**, 129 (2020).
[32] J. Liu, S. Meng, and J. T. Sun, Nano Lett. **19**, 3321 (2019).
[33] J. Liu, W. Hou, E. Wang, S. Zhang, J.-T. Sun, and S. Meng, Phys. Rev. B **100**, 081204(R) (2019).
[34] S. Kohler, J. Lehmann, and P. Hanggi, Phys. Rep. **406**, 379 (2005).
[35] N. Goldman and J. Dalibard, Phys. Rev. X **4**, 031027 (2014).
[36] M. Holthaus, J. Phys. B **49**, 013001 (2016).
[37] F. Meinert, M. J. Mark, K. Lauber, A. J. Daley, and H. C. Nagerl, Phys. Rev. Lett. **116**, 205301 (2016).
[38] J. Liu, W. Hou, L. Sun, X. Ma, X. Feng, T. Nie, and M. Zhao, J. Phys.: Condens. Matter **33**, 145701 (2021).
[39] O. V. Kibis, K. Dini, I. V. Iorsh, and I. A. Shelykh, Phys. Rev. B **95**, 125401 (2017).
[40] H. Hubener, M. A. Sentef, U. De Giovannini, A. F. Kemper, and A. Rubio, Nat. Commun. **8**, 13940 (2017).
[41] H. Liu, J.-T. Sun, and S. Meng, Phys. Rev. B **99**, 075121 (2019).
[42] M. Luo, Phys. Rev. B **99**, 075406 (2019).
[43] A. Kundu, H. A. Fertig, and B. Seradjeh, Phys. Rev. Lett. **116**, 016802 (2016).
[44] R. Bertoni, C. W. Nicholson, L. Waldecker, H. Hubener, C. Monney, U. DeGiovannini, M. Puppin, M. Hoesch, E. Springate, R. T. Chapman, C. Cacho, M. Wolf, A. Rubio, and R. Ernstorfer, Phys. Rev. Lett. **117**, 277201 (2016).
[45] M.-X. Guan, E. Wang, P.-W. You, J.-T. Sun, and S. Meng, Nat. Commun. **12**, 1885 (2021).
[46] U. De Giovannini, H. Hubener, and A. Rubio, Nano Lett. **16**, 7993 (2016).
[47] H. Liu, J. T. Sun, C. Cheng, F. Liu, and S. Meng, Phys. Rev. Lett. **120**, 237403 (2018).
[48] X. Kong, L. Li, L. Liang, F. M. Peeters, and X.-J. Liu, Appl. Phys. Lett. **116**, 192404 (2020).
[49] G. E. Topp, G. Jotzu, J. W. McIver, L. Xian, A. Rubio, and M. A. Sentef, Phys. Rev. Research **1**, 023031 (2019).
[50] See Supplemental Material at http://link.aps.org/supplemental/10.1103/PhysRevB.104.155439 for the derivation of the time-dependent effective Hamiltonian and the atomic and electronic structures of the BSb monolayer.
[51] H. Sahin, S. Cahangirov, M. Topsakal, E. Bekaroglu, E. Akturk, R. T. Senger, and S. Ciraci, Phys. Rev. B **80**, 155453 (2009).
[52] M. S. Rudner and N. H. Lindner, Nat. Rev. Phys. **2**, 229 (2020).
[53] G. Kresse and J. Furthmuller, Comput. Mater. Sci. **6**, 15 (1996).
[54] G. Kresse and J. Hafner, Phys. Rev. B **48**, 13115 (1993).
[55] R. D. King-Smith and D. Vanderbilt, Phys. Rev. B **47**, 1651 (1993).
[56] J. P. Perdew, K. Burke, and M. Ernzerhof, Phys. Rev. Lett. **77**, 3865 (1996).
[57] G. Kresse and J. Furthmüller, Phys. Rev. B **54**, 11169 (1996).
[58] G. Kresse and D. Joubert, Phys. Rev. B **59**, 1758 (1999).